A Multi-IMPATT Injection-Locked Oscillator at 35 GHz

MICHAEL G. ADLERSTEIN, SENIOR MEMBER, IEEE, AND JAMES FINES

Abstract—**A 35 GHz solid-state injection-locked oscillator giving 38 W peak power with 30 percent duty cycle is described. The power source utilizes a total of ten GaAs IMPATT diodes grouped in two stages. In this paper, we discuss the performance of the source as well as the systematic design and measurement procedures used to develop the multidiode cavities employed.**

I. Introduction

RECENT ADVANCES in demonstrated power and efficiency of pulsed GaAs IMPATT diodes [1], [2] have made possible the development of high-power pulsed solid-state millimeter-wave sources. In this paper, we describe the design and performance of a two-stage solid-state injection-locked oscillator giving 38 W peak power at 35 GHz.

The oscillator configuration is shown in Fig. 1. The first stage is an iris coupled two-diode rectangular Kurokawa cavity [3] and the second stage is an *E*-probe coupled eight-diode cylindrical TM_{020} Kurokawa cavity.

The source operated with a 500 ns pulse width and a 30 percent duty cycle. The locking bandwidth was 500 MHz, with locking gain of 13.3 dB at the highest output power point in the band. Overall dc to RF conversion efficiency was around 6 percent.

Cylindrical resonant cavity combiner structures were first described by Harp and Stover [4]. Many references to this type of structure are cited in a review paper by Chang and Sun [5]. Bayuk and Raue reported on a 37 GHz, 5 W amplifier using an eight-diode cylindrical resonant cavity [6]. Rectangular Kurokawa circuits have been used by a number of workers to combine the power of several IMPATT diodes in the millimeter-wave frequency bands [5], [7].

The development of the millimeter-wave cavities used in the amplifier reported here was conducted systematically. We employed a generalized *S*-parameter analysis, described in Section II and the Appendix. Once built, the cavities were characterized using an automatic network analyzer as described in Section II.

Locked oscillator performance is summarized in Section III. To our knowledge, the results presented here represent the highest combination of peak and average powers ever reported for such a source. However, we have not yet fully utilized the demonstrated capabilities of the high-power GaAs IMPATT diodes. We conclude that further circuit development work can lead to additional improvements in power source performance.

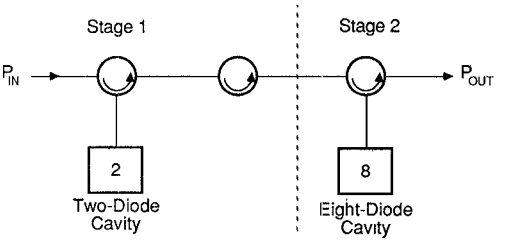

Fig. 1. Block diagram of two-stage locked oscillator.

II. Cavity Characterization

Systematic procedures were used to design the power-combining cavities. The general approach is to determine by measurement the load impedance for each diode at a fixed reference plane within the cavity. A large-signal model is used to calculate the diode impedance. Transformers near the diode are then selected to achieve the desired reflection gain.

Both the two-diode and the eight-diode cavity can be represented by the generalized network shown in Fig. 2. There are N equivalent diode ports and one input/output port. The S matrix describing this network is

$$[S] = \left[\begin{array}{c|c} S_{00} & S_{10}\cdots S_{10} \\ \hline S_{10} & \\ \vdots & [S']_{N\times N} \\ S_{10} & \end{array}\right] \tag{1}$$

where $[S']$ is "circulant." Each successive row of $[S']$ may be obtained from the preceding row by rotation. For example, if $N = 4$ and the symmetry of the structure is used to eliminate S_{14}, we have

$$[S'] = \begin{bmatrix} S_{11} & S_{12} & S_{13} & S_{12} \\ S_{12} & S_{11} & S_{12} & S_{13} \\ S_{13} & S_{12} & S_{11} & S_{12} \\ S_{12} & S_{13} & S_{12} & S_{11} \end{bmatrix} \tag{2}$$

Manuscript received March 11, 1988; revised October 20, 1988. This work was supported in part by the Naval Weapons Center, China Lake, CA, under Contract N60530-85-C-0261.

The authors are with the Research Division, Raytheon Company, 131 Spring St., Lexington, MA 02173.

IEEE Log Number 8825747.

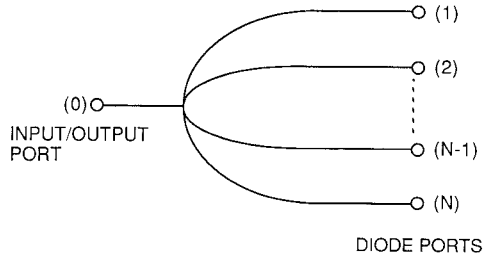

Fig. 2. Ports of a symmetrical power combiner.

It is shown in the Appendix that in terms of the above S parameters, such a power combiner can be represented as an equivalent two-port network with an S matrix given by

$$[S_e] = \begin{bmatrix} S_{00} & (\sqrt{N}\,S_{10}) \\ (\sqrt{N}\,S_{10}) & S_0 \end{bmatrix} \equiv \begin{bmatrix} S_{00} & S_t \\ S_t & S_0 \end{bmatrix} \tag{3}$$

where

$$S_0 = \sum_{n=1}^{N} S_{kn} \qquad (\text{any } k). \tag{4}$$

It is further shown in the Appendix that for equivalent diodes, each with reflection coefficient Γ_d, the termination on port 2 of the network described by (3) is also Γ_d. Thus, the reflection coefficient at port 1 (input/output) is

$$\Gamma_E = S_{00} + \frac{\Gamma_d S_t^2}{1 - S_0 \Gamma_d}. \tag{5}$$

The power gain is $|\Gamma_E|^2$.

The power added circuit efficiency, defined as

$$\eta_A = \frac{\text{net power added at port 1}}{\text{net power added at port 2}} \tag{6}$$

is

$$\eta_A = \frac{|S_{00} + \Gamma_d S_t F|^2 - 1}{|\Gamma_d F|^2 - |F|^2} \tag{7}$$

where

$$F = \frac{S_t}{1 - S_0 \Gamma_d}.$$

In the limit of infinite gain, the power added circuit efficiency approaches the oscillator efficiency for a multi-diode cavity [8]:

$$\eta_0 = \frac{|S_t|^2}{1 - |S_0|^2} = \frac{N|S_{01}|^2}{1 - \left| \sum_{n=1}^{N} S_{1n} \right|^2}. \tag{8}$$

Thus, if the IMPATT diode reflection coefficient is known, one can predict gain and power added circuit efficiency from measurements of S_t and S_0. Both S_t and S_0 can be determined by placing equivalent short circuits in all the diode ports and moving them simultaneously to at least three different reference planes while monitoring Γ_E. Equation (5) can then be solved for the equivalent two-port S parameters.

A useful representation of the gain for the power combiner may be obtained by plotting on the $1/\Gamma_d$ plane contours of constant $|\Gamma_E|$ which correspond to constant gain contours. By algebra, it can be shown that these contours are circles with centers at

$$\frac{1}{\Gamma_d} = S_0 + \frac{S_t^2}{S_{00}\left(|\Gamma_E/S_{00}|^2 - 1\right)} \tag{9a}$$

and with radii

$$\left| \frac{S_t^2 |\Gamma_E/S_{00}|}{S_{00}\left(1 - |\Gamma_E/S_{00}|^2\right)} \right|. \tag{9b}$$

It can further be shown that in the limit of a lossless circuit, the gain circle centers lie on a line between S_0 and the origin. For high-gain amplifiers, the gain circle centers are near S_0.

A. Dual-Diode Rectangular Cavity

The above analysis was applied to measurements made on the two-diode cavity used as the first stage of the locked oscillator. A schematic of the cavity is shown in Fig. 3(a), and a photo of the cavity built is shown in Fig. 3(b). The cavity is formed from a WR-22 waveguide section machined in a brass block. The waveguide is open at one end to allow termination in an adjustable short circuit. At the other end, half a guide wavelength away, the termination is provided by a coupling iris.

Penetrating the broad walls of the cavity are two gold-plated steel bias pins, nominally 0.032 in. in diameter. These pins are positioned symmetrically along the side walls of the waveguide. The RF currents driven in these pins by the IMPATT diodes couple power to the cavity. Each pin is terminated, on opposite sides of the block, in a matched tapered coaxial load. The IMPATT diodes and appropriate coaxial transformers of approximately 10 Ω impedance are mounted at the ends of the pins opposite the loads. By placing the diodes on different sides of the cavity, thermal "crosstalk," or mutual heating between the diodes, is minimized.

Fig. 4(a) shows the measured values of S_0. According to (5), S_0 represents the reflection coefficient to which each identical diode operating in phase must be matched by the transformers near the diode for the power-combining structure to operate as an oscillator.

The oscillator circuit efficiency calculated from (8) for the two-diode circuit is shown in Fig. 4(b). The best oscillator efficiency was around 80 percent and was obtained with irises having diameters in the range of 0.120 to 0.140 in. For larger irises, an excessive fraction of power available at the diode is lost in the coaxial load; for smaller irises, excessive power is dissipated in the cavity walls. The circuit efficiency is found to be very nearly constant over the 500 MHz band centered around 35 GHz. In fact, there is little change in oscillator efficiency for the optimum irises over the full 1 GHz band of the measurement.

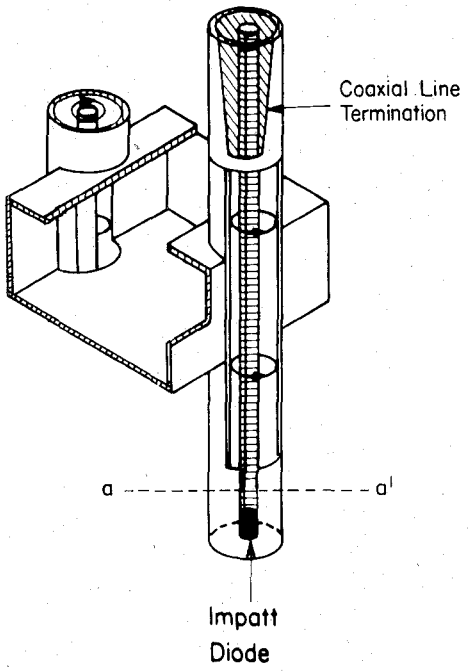

(a)

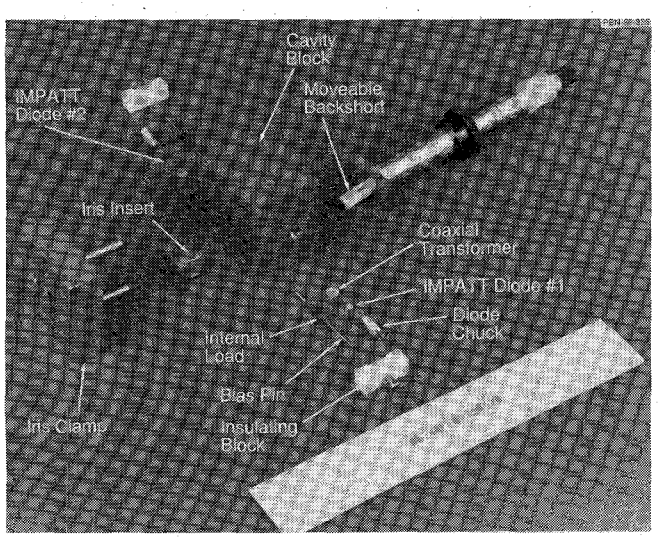

(b)

Fig. 3. (a) Two-diode waveguide cavity. (b) Two-diode cavity parts.

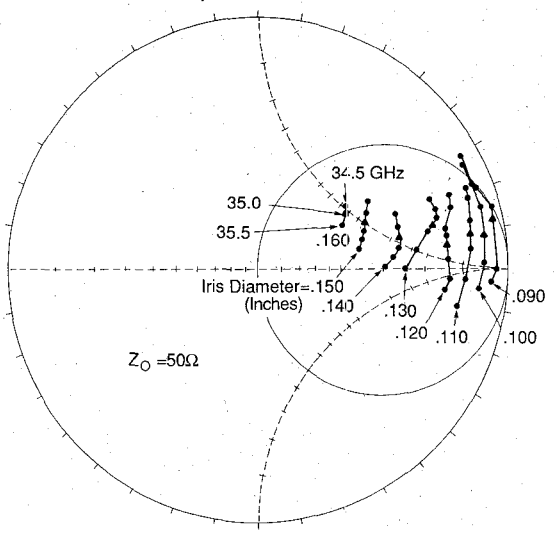

(a)

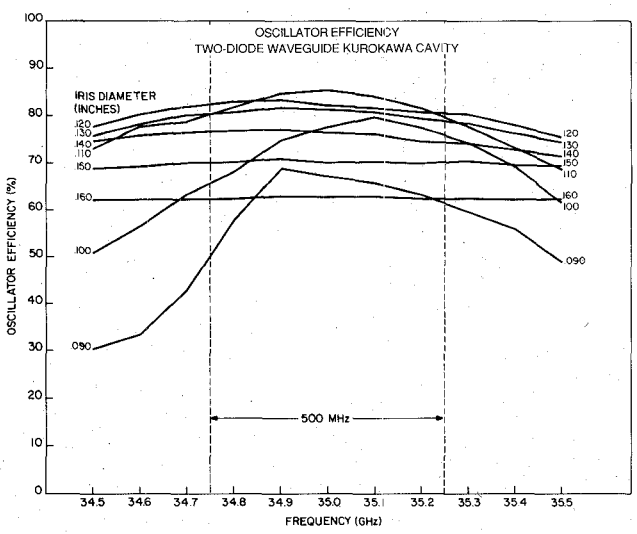

(b)

Fig. 4. (a) Measured S_0 for two-diode cavity with various irises. The reference plane is along the coaxial lines at the midplane of the cavity. (b) Measured oscillator efficiency for two-diode cavity using various irises.

The measured S parameters were used to calculate the expected amplifier response of the cavity from (9). Fig. 5 shows calculated contours of gain at 35 GHz and gives an indication of the changes in the 6 dB gain contour with frequency. Plotted for comparison is a calculated contour for $1/\Gamma_d$ versus frequency for 800 mW RF drive per diode. For the purpose of the calculation, we have used an analytical model of the IMPATT diode described elsewhere [9]–[11]. At any given frequency, the predicted gain is determined by the intersection of the $1/\Gamma_d$ point at that frequency and the gain contours at that frequency. The example in the figure predicts about 6 dB gain at 35.5 GHz and at 35.0 GHz with lower gain at 34.5 GHz.

Power added circuit efficiency contours calculated from (7) are shown in Fig. 6. It is evident that at the gain levels in the locked oscillator chain, the dual-diode cavity will be operating at nearly the full oscillator efficiency (around 75 percent).

B. Eight-Diode Cylindrical Cavity

As noted earlier, the second stage of the locked oscillator employs an eight-diode cylindrical TM_{020} cavity as the active module. A schematic representation of the cavity for the case of four diodes is shown in Fig. 7. Coaxial transmission lines are positioned in a radially symmetric pattern to excite the desired cylindrical cavity mode. Power is coupled out of the cavity through an E-probe inserted axially into the cavity. The E-probe is the center conductor of a coaxial transmission line which in turn couples to waveguide through a coax to WR-22 waveguide transition.

In addition to the E-probe, a dielectric tuner can be inserted axially from the opposite end of the cavity to

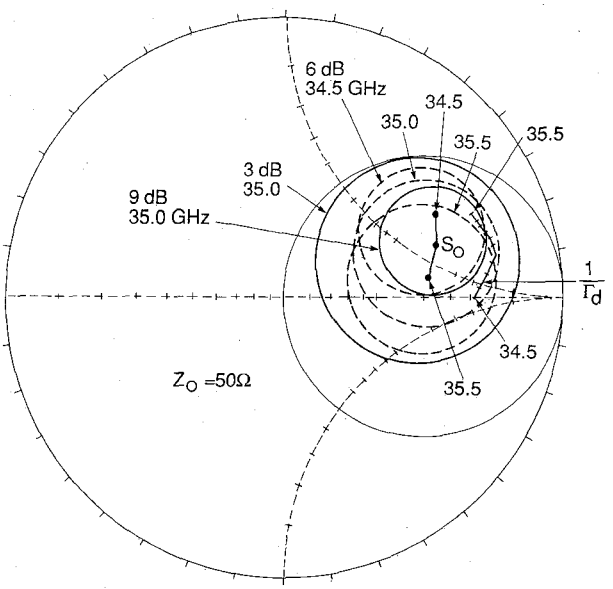

Fig. 5. Gain contours on the $1/\Gamma_d$ plane for the two-diode cavity. Diode $1/\Gamma_d$ is also shown. Diode parameters: $I_{dc}=1.9$ A, $A_j=1.5$E-4 cm^2, $P_{in}=0.8$ W/diode. Circuit parameters: 0.140 in. iris, 0.31 in. backshort, 0.168 in. 50 Ω spacer, 0.035 in. 35 Ω transformer.

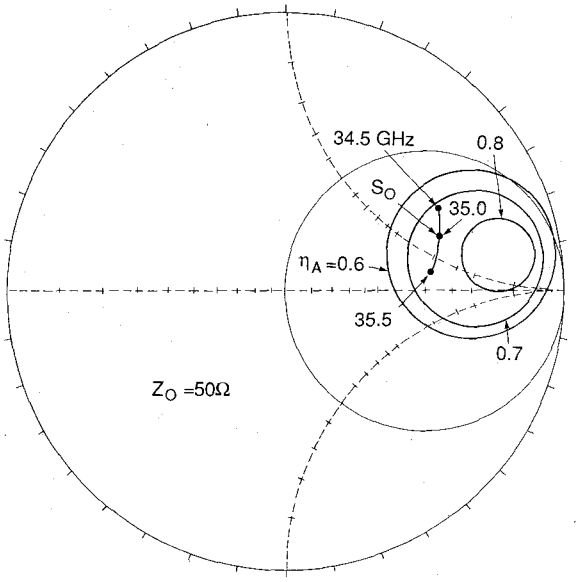

Fig. 6. Power added circuit efficiency contours on the $1/\Gamma_d$ plane for the two-diode cavity. Circuit parameters: $f=35$ GHz, 0.140 in. iris, 0.310 in. backshort.

adjust the resonant frequency. Thus, cavity adjustment of frequency and loading are roughly independent of each other.

The relationship between the S-matrix analysis given in the Appendix and the cylindrical cavity can be described in terms of the mode chart of Fig. 8. The chart relates the cavity resonant frequencies to cavity dimensions [12]. The modes of interest in the conventional cylindrical cavity are the TM_{0np} modes since, as shown in the Appendix, these can couple to the E-probe.

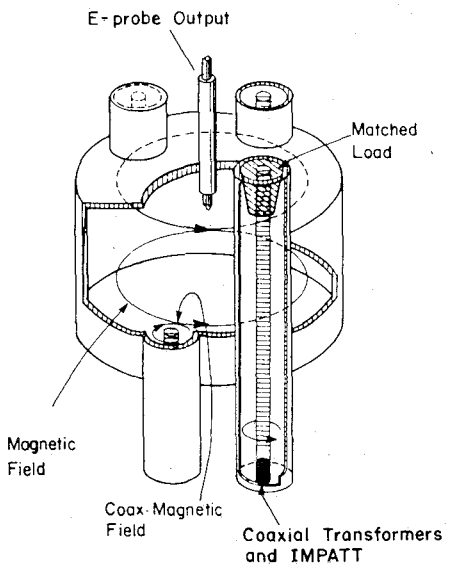

Fig. 7. Schematic representation of a four-diode cylindrical cavity combiner.

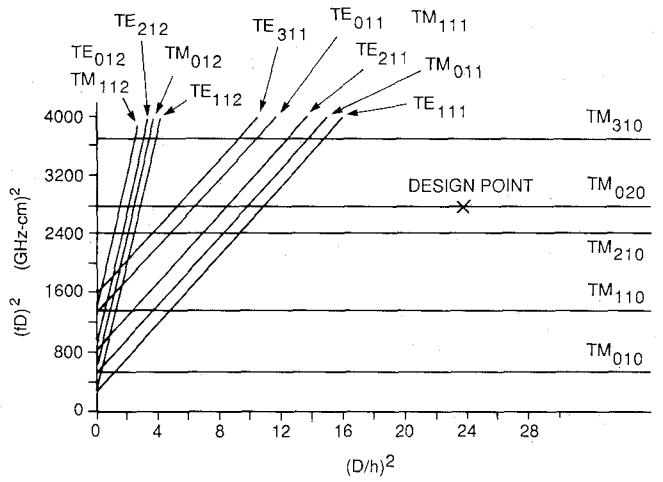

Fig. 8. Cylindrical cavity mode chart. D and h are the diameter and the height of the cavity respectively [12].

Compared with the TM_{010} mode at a given frequency, the TM_{020} mode has a larger associated cavity diameter and can accommodate more diode ports around the periphery. A diameter of 0.59 in. is obtained from the mode chart of Fig. 8. For the TM_{020} mode, however, there is a greater possibility of excitation of unwanted modes. The general condition for unwanted excitations is shown in the Appendix to be $\Gamma_d S_m=1$, where S_m is a "modal" S parameter. The values of S_m have their greatest variation with frequency near the resonant frequencies of the associated cavity modes.

To avoid possible excitation of the TE modes and others, the cavity height was chosen to be 0.12 in. The circumference of the cavity is 1.85 in., which is sufficient to accommodate the eight diodes and associated threads for mounting into the heat sink block. The most troublesome remaining unwanted mode is TM_{210}, whose reso-

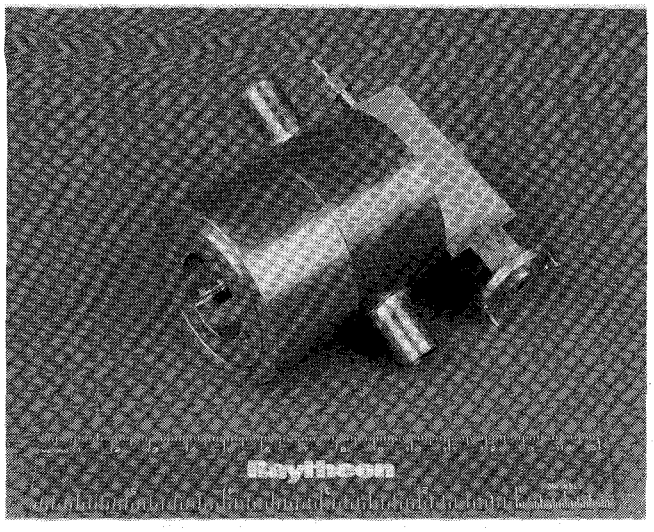

Fig. 9. TM_{020} eight-diode cavity.

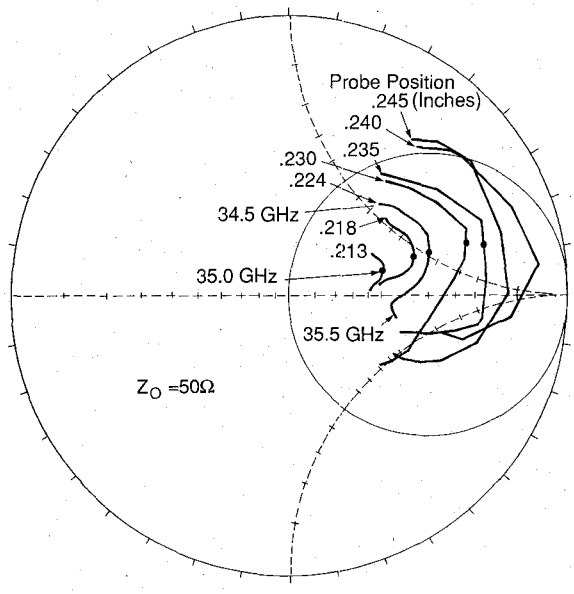

Fig. 10. S_0 at midplane for eight-diode TM_{020} cavity for various E-probe penetrations. No load spacers are used.

nance falls nearest that of TM_{020} at the cavity design point shown in Fig. 8. The unwanted mode may be suppressed by appropriately loading the cavity [13].

The design principles discussed above were used to construct the eight-diode TM_{020} cavity shown in Fig. 9. The coaxial lines used in the cavity are similar to those employed in the two-diode first stage: diode and transformer combinations may be used interchangeably in either cavity.

As was done for the two-diode circuit, we carried out measurements of the even-mode S parameters for the TM_{020} circuit. Eight sets of identical coaxial offset short circuits were used in the diode lines. The reflection coefficient at the waveguide port was measured with the automatic network analyzer after first setting the dielectric tuner to resonate the cavity at 35 GHz. The cavity resonant frequency was defined as that frequency where S_0 at the cavity midplane crosses the real axis of the Smith chart. The tuner setting was determined crudely using three (the minimum number) short circuit sets. A full measurement using nine short circuit sets was then carried out.

Measured values over a 1 GHz band of S_0 are shown in Fig. 10. As expected, the curves move radially with E-probe insertion, rendering E-probe insertion the primary gain adjustment.

Oscillator efficiency can be calculated as was done for the two-diode cavity. The results are plotted in Fig. 11. The maximum oscillator efficiency obtained was around 72 percent midband, falling off to 40 percent at the band edges. Measurement of unloaded cavity Q indicted a value of around 2200, so that we were not experiencing excessive losses in the cavity walls. Most of the power available at the diode ports not appearing at the output port was being dissipated in the coaxial terminating loads.

Based on the S-parameter measurements described above, the gain and power added circuit efficiency contours for the even mode of the eight-diode cavity were

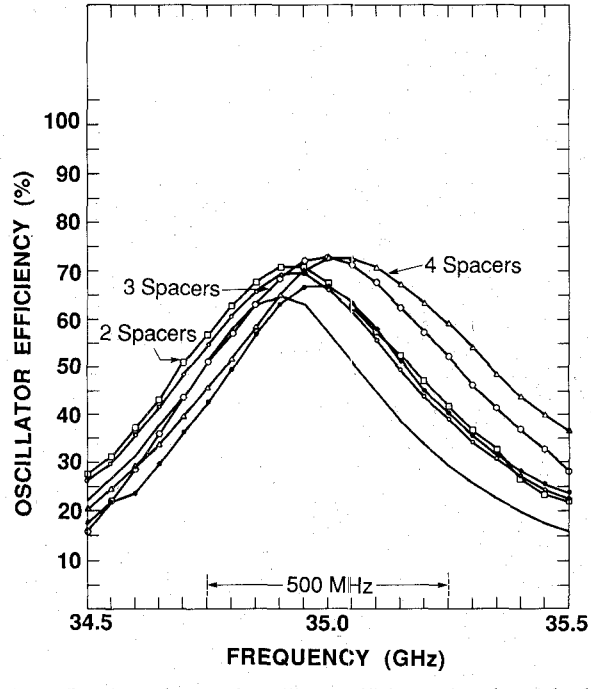

Fig. 11. The dependence of oscillator efficiency for the eight-diode TM_{020} cavity on placement of the coaxial loads. Each spacer has a thickness of 0.018 in. E-probe penetration is 0.325 in.

calculated. The results are shown for 35 GHz in Fig. 12 plotted on the $1/\Gamma_d$ plane. In the region to the right of S_0 (the point of infinite gain), gain and power added circuit efficiency contours are coincident. Between 6 and 9 dB gain, the power added circuit efficiency is seen to be between 65 and 70 percent.

It would certainly be desirable to increase the power added circuit efficiency. It may be possible to improve this efficiency by using flat-faced loads having a significant mismatch to the coaxial line. This must be done without

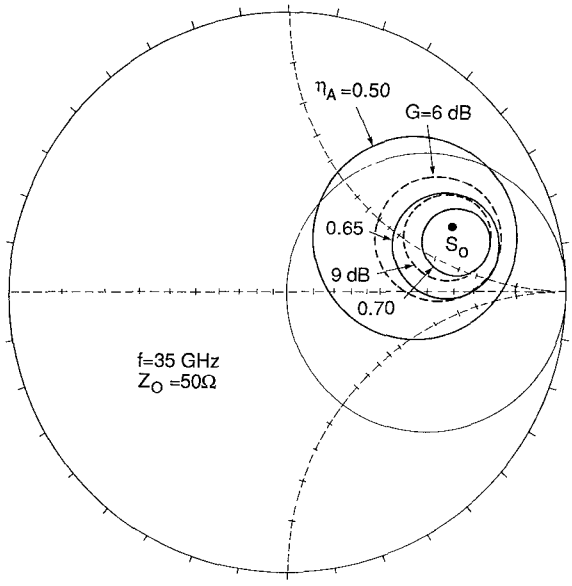

Fig. 12. Calculated gain and power added circuit efficiency contours on the $1/\Gamma_d$ plane for the eight-diode TM_{020} cavity. The E-probe is set at 0.230 in. penetration and four load spacers are used.

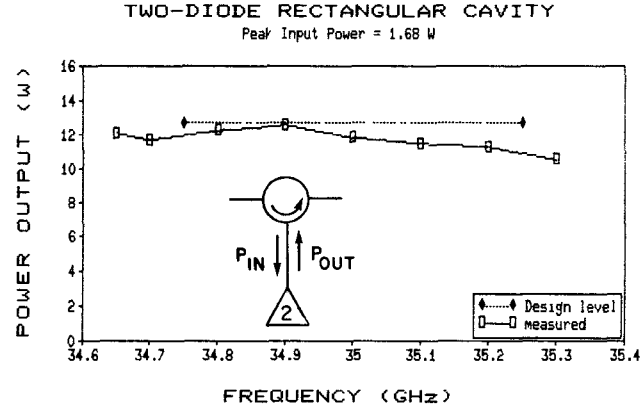

Fig. 13. Swept frequency measurements of the two-diode cavity.

unduly sacrificing bandwidth or diode stability. The efficiency might be improved further by increasing the efficiency of the waveguide to coaxial transition from its measured value of 90 percent.

III. Cavity Performance

All GaAs IMPATT diodes used in the power source were fabricated in our laboratory. Diodes operate at approximately 2 A, peak bias current at around 30 V. The waveform was 500 ns pulsed at 30 percent duty cycle. The RF performance obtained may be summarized as follows.

A. Dual-Diode Cavity

The two-diode waveguide Kurokawa circuit was evaluated in swept-frequency amplifier tests. The results are shown in Fig. 13. Input power at the cavity flange was 1.68 W. Peak output power is between 11 and 12 W across the test range.

There was no observable frequency chirp during the pulse. The spectral purity was such that, at high resolution,

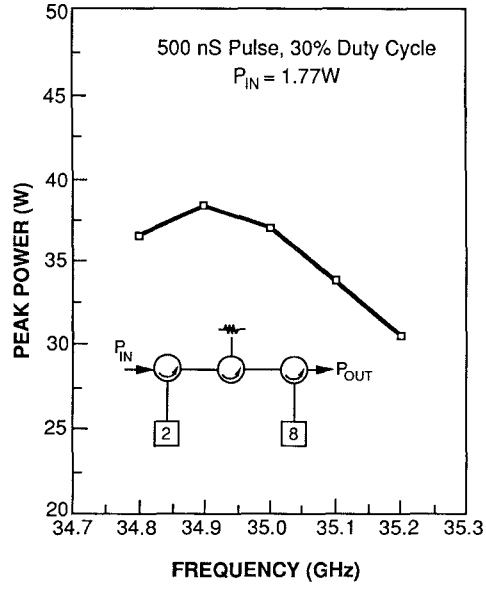

Fig. 14. Two-stage pulsed IMPATT amplifier performance.

the Fourier components of the pulsed waveform were clearly visible on the spectrum analyzer. Noise sidebands observed 20 dB below the carrier were caused by feedthrough of noise from the TWT exciter.

B. Eight-Diode TM_{020} Cavity

Using the gain and efficiency contours shown in Fig. 12, we designed a set of coaxial transformers to test the eight-diode cylindrical cavity. Diodes were selected based on the results of single diode evaluation. In the qualification process, diodes were paired with particular coaxial transformers. This combination was used together in the cylindrical cavity. A minimum power output level of 7 W peak at 30 percent duty cycle was required of the diodes for qualification. Diodes which operated with similar tuning at similar frequencies giving similar power output were grouped. It was found to be possible to use simultaneously in the cavity diodes from several different wafers.

The dual-diode stage was used with an intervening attenuator to drive the eight-diode stage tuned as a 35 GHz oscillator with maximized power output. At the eight-diode cavity flange, output power varied smoothly with drive from 31 W with zero input power to 35 W with 3 W of drive. Output power remained saturated between 3 and 5 W of drive.

In conducting the tests, the dual-diode stage was triggered 20 to 30 ns prior to triggering the bias on the eight-diode cavity. Such pretiming of the stages resulted in a faster rise time for the RF output of the amplifier.

Swept-frequency measurements are summarized in Fig. 14. The cavities were retuned to give maximum power over a 500 MHz band with 1.77 W input. Maximum power was obtained in the low-frequency portion of the band, an effect most likely due to a relative angle between $1/\Gamma_d$ and S_0 on the $1/\Gamma_d$ plane. Frequency lock was lost beyond the band edges at the input power provided.

TABLE I
TWO-STAGE LOCKED OSCILLATOR OPERATING SUMMARY*

	Stage 1	Stage 2
Diodes per stage	2	8
Gain at cavity flange (dB)	8.0	6.3
Input power to stage (W)	1.77	9.72
Input power at cavity (W)	1.69	9.28
Power added at chip (W)	6.14	5.19
Power added at cavity (W)	8.97	30.33
Power output of stage (W)	9.72	37.84

*See Fig. 1 for definition of stages.
$f = 35$ GHz.
Nominal power added circuit efficiency = 73 percent.
Circulator loss = 0.2 dB.

To assess the performance of the locked oscillator relative to measured performance levels of individual diodes, we have used results of the S-parameter analysis to track the power flow within the RF chain as shown in Table I. Here, we have taken into account not only the losses in the RF chain but also the inherent power added circuit efficiency of the Kurokawa cavities. It was found that each of the two IMPATT diodes in the first stage added approximately 5.6 W peak at 10 percent dc to RF conversion efficiency. Those in the eight-diode cavity added 4.7 W at 8 percent dc to RF conversion efficiency. Since each of the ten diodes used in the locked oscillator gave 7 W peak at 13 percent efficiency in single diode tests, it is likely that we have not yet achieved optimum diode match in the multidiode cavity. Improved performance with further circuit refinements can be expected.

IV. CONCLUSIONS

A systematic design and analysis procedure for multi-IMPATT diode cavities has been presented. The procedures have been applied to the development of a dual-diode rectangular Kurokawa cavity and an eight-diode cylindrical TM_{020} cavity. In a two-stage configuration, 38 W peak power was achieved at 35 GHz. Average power was around 12 W. Similar performance was obtained when the source was operated as a locked oscillator with 500 MHz bandwidth.

Further work will be required to extract the full available power of the GaAs IMPATT diodes. This work must involve improving the power added circuit efficiency of the cavities as well as providing improved matching to the diode chips.

APPENDIX

The S-parameter relations used in the foregoing sections may be derived by describing the input and output waves at the ports shown in Fig. 2 in terms of column vectors α and β, which are related by the scattering matrix equation $\beta = [S]\alpha$.

Consider the eigenvectors of $[S']$ of equation (1) defined by the vector equation

$$[S']\boldsymbol{x}_m = S_m \boldsymbol{x}_m \tag{A1}$$

where S_m is a constant. The column vectors $\boldsymbol{x}_m$ have the normalized form

$$\boldsymbol{x}_m = \frac{1}{\sqrt{N}} \begin{pmatrix} 1 \\ e^{jm\gamma} \\ e^{j2m\gamma} \\ \vdots \\ e^{j(N-1)m\gamma} \end{pmatrix} \tag{A2}$$

where $\gamma = 2\pi/N$ and $m = 0, 1, \cdots, N-1$. The associated eigenvalues are

$$S_m = \sum_{n=1}^{N} S'_{1n} e^{j(n-1)m\gamma}. \tag{A3}$$

The number of distinct eigenvalues is the same as the number of distinct values of S'_{1n}, which is $(N/2)+1$ for N even and $(N+1)/2$ for N odd.

Define the $N+1$ by $N+1$ matrix $[X]$ shown below:

$$[X] = \begin{bmatrix} 1 & 0 & 0 & \cdots & 0 \\ 0 & & & & \\ 0 & & & & \\ \vdots & \boldsymbol{x}_0 & \boldsymbol{x}_1 & \cdots & \boldsymbol{x}_{N-1} \\ 0 & & & & \end{bmatrix} \tag{A4}$$

The inverse of $[X]$ is the transposed complex conjugate of $[X]$, denoted by $[X]^{-1}$.

Taken as vectors, the columns of the matrix $[X]$ form an orthonormal basis. Any possible set of inputs from the diode ports can be expressed as a linear combination of these vectors. The coefficient of each vector is considered to be the wave excitation of the associated "modal port."

Consider again the scattering equation $\beta = [S]\alpha$. This is equivalent to

$$\boldsymbol{b} = [S_M]\boldsymbol{a} \tag{A5a}$$

where

$$\boldsymbol{b} = [X]^{-1}\beta \qquad \boldsymbol{a} = [X]^{-1}\alpha$$

and

$$[S_M] = [X]^{-1}[S][X] \tag{A5b}$$

so that

$$[S_M] = \left[\begin{array}{cc|ccc} S_{00} & (\sqrt{N}\,S_{10}) & & 0\cdots 0 & \\ (\sqrt{N}\,S_{10}) & S_0 & & & \\ \hline & & S_1 & & \\ 0 & & & S_2 & \\ \vdots & & & & \ddots \\ 0 & & & & S_{N-1} \end{array}\right] \tag{A6}$$

The matrix $[X]^{-1}$ transforms the power flow from the diode port basis to the modal port basis.

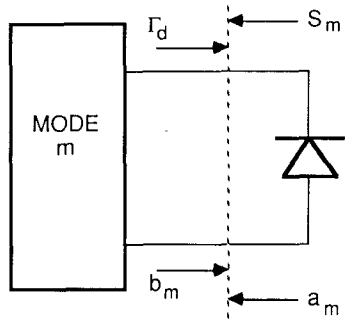

Fig. 15. Waves and termination for the modes with $m > 0$.

If a power wave α enters the diode ports, then the total power entering the network is the vector dot product, $\alpha^* \cdot \alpha$. Likewise, the total power entering the network in the "modal" representation can be expressed as

$$\boldsymbol{a}^* \cdot \boldsymbol{a}. \tag{A7}$$

Consider, for example, identical waves of amplitude α entering each diode port. Expressed in the modal basis we have

$$\boldsymbol{a} = [X]^{-1}\alpha. \tag{A8}$$

The total power input in either basis remains $N|\alpha|^2$, as it must. The power flowing into the mth mode is $|a_m|^2$, where a_m is the mth entry in the modal column vector.

The form of the S matrix in the modal representation shows that there is isolation between the N modes. Also, there is no coupling between modes 1 through $N-1$ and the output port. This corresponds to phase cancellation at the output port of the waves entering the diode ports. Mode 0, referred to as the even mode, does couple to the output.

Let the reflection coefficient at each diode port looking toward the diode be Γ_d. Γ_d would be the reflection coefficient of the semiconductor chip transformed by the intervening circuitry. Generally, $|\Gamma_d| > 1$. If β is the wave incident on the diode port terminations, then the reflected wave is $\alpha = \Gamma_d \beta$. In the modal representation, we have

$$\boldsymbol{a} = [X]^{-1}\alpha = [X]^{-1}\Gamma_d\beta = \Gamma_d[X]^{-1}\beta = \Gamma_d \boldsymbol{b} \tag{A9}$$

so that the reflection coefficient of the modal wave is the same as that of the termination on each diode port.

Although the modes $m = 1$ to $N-1$ do not couple to the output port of the cavity, IMPATT diodes have broad-band negative resistance and can deliver power into these modes under certain conditions. Each of these modes can be considered to be a one-port termination of the active elements, as shown in Fig. 15.. The equations governing the termination are

$$\begin{aligned} b_m &= S_m a_m \\ a_m &= \Gamma_d b_m \end{aligned} \tag{A10}$$

which show a sustained oscillation if $\Gamma_d S_m = 1$. Thus, to avoid oscillation, $1/\Gamma_d$ should be adjusted to avoid the above condition at all frequencies.

For the cylindrical cavity, there is a relationship between the modes in Fig. 8 and the N modes discussed above. For example, the angular symmetry of the transverse magnetic modes is given by the first index, q, in the mode designation TM_{qnp}. Any excitation of a modal port with index m must involve a linear combination of cavity mode solutions with

$$\begin{aligned} q &= m + kN \qquad \text{for } m = 0,1,2,\cdots,N-1 \\ &\qquad\qquad \text{with } k = 0,1,\cdots. \end{aligned} \tag{A11}$$

It is not a simple matter to determine the values of S_m for $m > 0$ due to the isolation of the output port from these modes. One approach is to measure the diode port-to-diode port S parameters through appropriate transitions and construct S_m by diagonalizing the resulting S matrix using $[X]^{-1}$.

For the two cavities used in the present case, we have not measured S_m, but have ensured that the unwanted modes are sufficiently removed from the operating frequency so that they do not affect cavity operation.

The two ports consisting of the even mode and the output have all the properties of a standard two-port network. The S matrix describing this network is the upper left submatrix of (A6) as used in equation (3).

Acknowledgment

The authors acknowledge the contributions of their many colleagues, particularly R. Carvalho and D. Argentini. They also thank M. Afendykiw of NWC, J. Caufmann of the Office of Naval Technology, and A. Glista of the Naval Air Systems Command for their support and encouragement.

References

[1] M. G. Adlerstein and S. L. G. Chu, "GaAs IMPATT diodes pulsed at 40 GHz," in *Proc. Int. Microwave Symp.* (San Francisco, CA), 1984, pp. 481–482.

[2] M. G. Adlerstein *et al.*, "High efficiency *Ka*-band GaAs pulsed IMPATT diode development," Raytheon Research Division Final Report to Naval Weapons Center, China Lake, CA, Contract N60530-85-C-0239, Sept. 1986.

[3] K. Kurokawa, "The Single-Cavity Multiple Device Oscillator," *IEEE Trans. Microwave Theory Tech.*, vol. MTT-19, pp. 793–801, Oct. 1971.

[4] R. S. Harp and H. L Stover, "Power combining of *X*-band IMPATT circuit modules," in *1973 IEEE-ISSCC Dig Tech. Papers*, vol. XVI, Feb. 1973, pp. 118–119.

[5] K Chang and C. Sun, "Millimeter-wave power-combining techniques," *IEEE Trans Microwave Theory Tech.*, vol. MTT-31, pp. 91–107, Feb. 1983.

[6] F. J. Bayuk and J. Raue, "Ka-band solid state power amplifier," in *1977 IEEE MTT-S Symp. Dig.*, pp. 29–35.

[7] D. W. Mooney and F. J. Bayuk, "41-GHz 10-Watt solid-state amplifier," in *Proc. 11th European Microwave Conf.* (Amsterdam), Sept. 1981, pp. 876–881.

[8] D. M. Kinman, D. J. White, and M. Afendykiw, "Symmetrical combiner analysis using *S*-parameters," *IEEE Trans. Microwave Theory Tech.*, vol. MTT-30, pp. 268–277, Mar. 1982.

[9] M. G. Adlerstein and E. Moore, in *Proc. 8th Biennial Conf. Active Microwave Semiconductor Devices* (Cornell University), 1981, pp. 375–384.

[10] D Masse *et al.*, "Millimeter-wave GaAs IMPATT diodes," *Infrared and Millimeter-waves*, vol. 14 New York: Academic Press, 1985 pp. 291–370.

[11] M. Cobb, Private communication.

[12] C. G. Montgomery, *Technique of Microwave Measurements* (MIT Radiation Lab Series, vol. 11) Lexington, MA: Boston Technical Lithographers, 1963, pp. 297–303.

[13] C. A. Drubin *et al.*, "A 1 kW peak, 300 W average IMPATT diode injection-locked oscillator," in *1982 IEEE MTT-S Dig.*, pp. 126–128.

✠

Michael G. Adlerstein (SM'81) is a Consulting Scientist at the Raytheon Company, Lexington, MA. He received the B.S. degree (summa cum laude) in mathematics and the M.S. degree in physics simultaneously in 1966 from the Polytechnic Institute of Brooklyn, Brooklyn, NY. He received the Ph.D. degree and a second master's degree in 1971 in applied physics from Harvard University, Cambridge, MA. During a portion of his doctoral work he was a Visiting Scientist at the Francis Bitter National Magnet Laboratory of the Massachusetts Institute of Technology.

Since joining the Research Division of the Raytheon Company in 1971, he has worked in the field of microwave and millimeter-wave semiconductor device research.

Dr. Adlerstein served as Associate Editor for Microwave Devices of the IEEE TRANSACTIONS ON ELECTRON DEVICES (1981–1983) and currently is Publications Chairman of the Cornell University High Speed Electron Device Conference Committee. He is a Life Member of the American Physical Society, Sigma Xi, Sigma Pi Sigma, and Pi Mu Epsilon.

✠

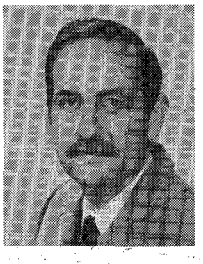

James Fines was born in Amarillo, TX, in September 1947. He received the B.S. and Ph.D. degrees from the Massachusetts Institute of Technology in 1969 and 1980, respectively.

He joined the Research Division of the Raytheon Company in 1980, where he worked on circuits for power-combining millimeter-wave IMPATT diodes. He is now engaged in developing techniques for the microwave characterization of the new, high-temperature superconductors.

Dr. Fines is a member of the American Physical Society and Sigma Xi.